RSC Advances

PAPER

View Article Online
View Journal | View Issue

Cite this: *RSC Adv.*, 2023, **13**, 23984

$[Cs©C_{18}]^+$ and $[Na©C_{14}]^+$: perfect planar alkaline-metal-centered polyynic cyclo[*n*]carbon complexes with record coordination numbers†

Min Zhang, Rui-Nan Yuan, Yan-Bo Wu, Qiang Chen, Zhihong Wei and Si-Dian Li *

Received 12th June 2023
Accepted 4th August 2023

DOI: 10.1039/d3ra03930g

rsc.li/rsc-advances

Searching for the maximum coordination number (CN) in planar species with novel bonding patterns has fascinated chemists for many years. Using the experimentally observed polyynic cyclo[18]carbon D_{9h} C_{18} and theoretically predicted polyynic cyclo[14]carbon D_{7h} C_{14} as effective ligands and based on extensive first-principles theory calculations, we predict herein their perfect planar alkaline-metal-centered complexes D_{9h} $Cs©C_{18}^+$ (**1**) and D_{7h} $Na©C_{14}^+$ (**4**) which as the global minima of the systems possess the record coordination numbers of CN = 18 and 14 in planar polyynic species, respectively. More interestingly, detailed energy decomposition and adaptive natural density partitioning bonding analyses indicate that the hypercoordinate alkaline-metal centers in these complexes exhibit obvious transition metal behaviors, with effective in-plane (π-6s)σ, (π-7p)σ, and (π-5d)σ coordination bonds formed in $Cs©C_{18}^+$ (**1**) and (π-3s)σ, (π-3p)σ, and (π-3d)σ coordination interactions fabricated in $Na©C_{14}^+$ (**4**) to dominate the overall attractive interactions between the metal center and its cyclo[*n*]carbon ligand. Similarly, alkaline-metal-centered planar C_s $Cs©C_{17}B$ (**2**), C_{2v} $Cs©C_{17}^-$ (**3**), C_{2v} $Na©C_{13}B$ (**5**), and C_{2v} $Na©C_{13}^-$ (**6**) have also been obtained with CN = 18, 17, 14, and 13, respectively.

1 Introduction

The successive discoveries of fullerenes in 1985,[1] carbon nanotubes in 1991,[2] and graphene in 2004 [3] which all consist exclusively of 3-coordinate carbon atoms have sparked a new field of synthetic carbon allotropes in chemistry. The recent characterization of polyynic cyclo[18]carbon D_{9h} C_{18} with bond length alternation (BLA) in 2019 using high-resolution atomic force microscopy marked the onset of an alternative family of molecular carbon allotropes consisting solely of 2-coordinate carbon atoms in the C_{4N+2} cyclo[*n*]carbon ring series.[4] Previous gas-phase experiments indicated that cyclo[*n*]carbon rings as primary precursors may coalescence to form fullerenes and carbon nanotubes.[5,6] Electronic spectroscopic measurements showed that both C_{18} and C_{14} possess monocyclic geometries, though these studies did not reveal whether they have cumulantic or polyynic structures.[7,8] High level quantum Monte Carlo (QMC) simulation and coupled cluster methods with single and double excitations (CCSD) investigations indicated that both polyynic D_{9h} C_{18} and D_{7h} C_{14} are the ground states of the systems due to second-order Jahn-Taller effects, with their cumulantic counterparts with no BLA always behaving as transition states.[9,10] Such perfect monocyclic $D_{(2N+1)h}$ C_{4N+2} polyynic species have aroused considerable interests among chemists and presented viable possibilities to form planar metal-doped cyclo[*n*]carbon complexes with super-high coordination numbers (CN). A recent theoretical investigation[11] suggested that the Li-doped C_{18} complex may serve as a potential optical switch which transforms between two stable C_s configurations with Li inside ($Li@C_{18}^{in}$) and outside the carbon ring ($Li@C_{18}^{out}$). However, in the ground state ($Li@C_{18}^{in}$) of such an alkaline-metal-doped cyclo[18]carbon complex, the Li atom with the coordination number of CN = 5 appears to be severely off-centered due to the size mismatch between Li and its monocyclic C_{18} ligand. Similar situation happens in the recently proposed metal-doped $M@C_{16}$ complexes (M = Ca, Sc, Ti, V, Ce, U) in which the off-centered alkaline-earth, lanthanide, or actinide metal atoms have the coordination numbers between CN = 4 ∼ 6,[12] again due to size effect. A recent first-principles theory investigation by our group indicated that, in the experimentally observed $La©C_{13}^+$, the La center with the large atomic radius of r_{La} = 1.83 Å [13] matches the C_{13} ligand perfectly both geometrically and electronically to form the perfect planar La-centered D_{13h} $La©C_{13}^+$ which has the highest coordination number of CN = 13 in planar species reported to date, demonstrating the unique coordinating capability of cyclo[*n*]carbon rings as effective ligands to metal centers in chemistry.[14]

Shanxi University, China. E-mail: lisidian@sxu.edu.cn; weizhihong@sxu.edu.cn; chenqiang@sxu.edu.cn

† Electronic supplementary information (ESI) available. See DOI: https://doi.org/10.1039/d3ra03930g

However, it still remains unknown to date in both experiments and theory whether or not metal-centered hypercoordinate planar cyclo[*n*]carbon complexes with CN > 13 can be achieved in chemistry. To achieve higher CNs (CN = $n \geq 14$) in metal-centered cyclo[*n*]carbon complexes, it requires in chemical intuition that the metal centers have atomic radii greater than that of La.

Searching for the maximum coordination number in planar species is more than a curiosity, it is to push the limits and ultimately to understand the essential concepts in chemistry.[14,15] To successfully design a metal-centered hypercoordinate planar complex, the metal center and its ligand must match both geometrically and electronically, *i.e.*, they must have the right geometrical sizes and electronic configurations. The prototypical electron-deficient planar cyclo[*n*] boron rings have proven to be effective ligands to coordinate transition metal centers. Perfect σ + π dually aromatic wheel-like D_{8h} Co©B_8^-, D_{9h} Ru©B_9^-, D_{9h} Rh©B_9^-, D_{9h} Ir©B_9^-, D_{10h} Ta©B_{10}^-, and D_{10h} Nb©B_{10}^- with CN = 8, 9, 9, 9, 10, and 10 have been observed in gas phases in recent joint photoelectron spectroscopy and first-principles theory investigations.[15–20] These results present the possibility to form metal-centered hyper-coordinate planar complexes using C_nB_m binary monocyclic rings as effective ligands, as indicated in the cases of the previously reported C_{2v} Y©$B_6C_6^+$ and C_{2v} Sc©B_5C_6.[14]

Alkaline-earth metal centers in their perfect body-centered cubic carbonyl complexes O_h M$(CO)_8^+$ (M = Ca, Sr, or Ba) in low-temperature neon matrixes have been confirmed to be honorary transition metals with effective M–$(CO)_8$ (π) coordination interactions.[21] Similar M(d_π)–$(CO)_8$ (π) coordination bonds were predicted to exist in O_h M$(CO)_8^-$ complexes (M = K, Rb) in which the alkaline metal centers K and Rb exhibit transition metal behaviours.[22] Given the fact that alkaline metals possess the largest atomic radii in the periodical table[23] and have the potential to form complexes with transition metal behaviors, it is possible to form alkaline-metal-doped cyclo[*n*] carbon complexes ($n \geq 14$) or their boron-substituted derivatives with CN ≥ 14 if the alkaline metal center and its ligand are chosen properly to match both geometrically and electronically.

Keeping the inspirations in mind, using the experimentally observed perfect planar ring-like D_{9h} C_{18} and theoretically predicted D_{7h} C_{14} as ligands and based on extensive global minimum searches augmented with first-principles theory calculations, we predict in this work the perfect planar alkaline-metal-centered D_{9h} Cs©C_{18}^+ (**1**) and D_{7h} Na©C_{14}^+ (**4**) which have the record coordination numbers of CN = 18 and 14 in planar species, respectively. Cs and Na with the atomic radii of r_{Cs} = 2.65 Å and r_{Na} = 1.86 Å [13] prove to match the D_{9h} C_{18} and D_{7h} C_{14} ligands perfectly both geometrically and electronically, respectively. Effective in-plane (π-s)σ, (π-p)σ, and (π-d)σ coordination bonds are formed to dominate the attractive interactions in these novel complexes in which the alkaline-metal centers exhibit transition metal behaviors. The iso-chemical shielding surfaces and out-of-plane π and in-plane σ ring current maps of the concerned species are computationally simulated to evidence their σ + π dual aromaticity.

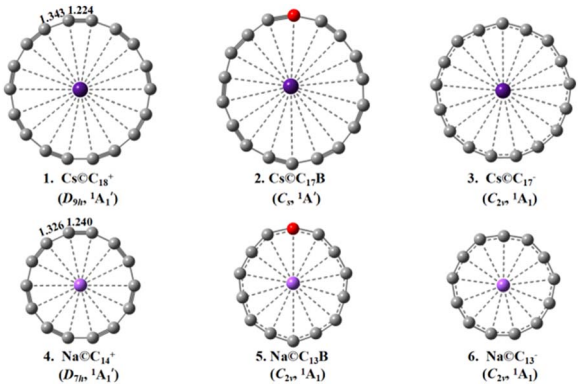

Fig. 1 Optimized structures of D_{9h} Cs©C_{18}^+ (**1**), C_s Cs©C_{17}B (**2**), C_{2v} Cs©C_{17}^- (**3**), D_{7h} Na©C_{14}^+ (**4**), C_{2v} Na©C_{13}B (**5**), and C_{2v} Na©C_{13}^- (**6**) at M06-2X level.

2 Computational details

Extensive global-minimum (GM) searches were performed on Cs©C_{18}^+, Na©C_{14}^+, Cs©C_{17}B, Cs©C_{17}^-, Na©C_{13}B, and Na©C_{13}^- using the TGmin2 code[24] at DFT level based on the basin-hopping algorithm.[25] Over 1000 stationary points were explored for each species at PBE/DZVP level employing the CP2K program.[26,27] The low-lying isomers were then fully optimized at both M06-2X and ωB97XD levels[28,29] with vibrational frequencies checked, with the aug-cc-pvtz basis set for C, B, Na, and K and Stuttgart relativistic small-core pseudopotentials[30,31] for Rb, Cs, and Fr, using the Gaussian16 program.[32] The fact that M06-2X produces essentially the same polyynic D_{9h} C_{18} and D_{7h} C_{14} structures (Fig. S1†) as that obtained at the more accurate QMC and CCSD levels[9,10] evidences the reliability of the optimized geometries depicted in Fig. 1. Natural bond orbital (NBO) analyses were performed using NBO 7.0 program.[33] The energy decomposition analyses (EDA) together with the natural orbitals for chemical valence (NOCV) calculations, denoted as EDA-NOCV,[34–36] were carried out with the ADF program package[37] at M06-2X/TZ2P[38] level where scalar relativistic effects were considered for Cs using the zero order regular approximation (ZORA).[39] The frozen core approximation was not employed in EDA-NOCV computations. The overall interaction energy (ΔE_{int}) between two fragments is divided into three main terms: the electrostatic interaction energy (ΔE_{elstat}), Pauli repulsion (ΔE_{Pauli}), and orbital interaction energy (ΔE_{orb}) in eqn (1):

$$\Delta E_{int} = \Delta E_{elstat} + \Delta E_{Pauli} + \Delta E_{orb}. \quad (1)$$

Detailed bonding analyses on D_{9h} Cs©C_{18}^+ (**1**), D_{7h} Na©C_{14}^+ (**4**), and C_s Cs©C_{17}B (**2**) were implemented using the adaptive natural density partitioning (AdNDP 2.0) approach[40,41] at the M06-2X/6-31G level, with the isosurface maps of the orbitals visualized using the Visual Molecular Dynamics (VMD) software.[42] The iso-chemical shielding surfaces (ICSSs)[43,44] and isosurfaces of localized orbital locators (LOL)[45] were obtained with Multiwfn 3.8 code.[46] The anisotropy of the current-induced

density (ACID) analyses were realized by the ACID code,[47] with the maps finally generated by POV-Ray render.[48]

3 Results and discussions

3.1 Structures and stabilities

The optimized GM structures of D_{9h} Cs©C_{18}^+ (**1**), C_s Cs©C_{17}B (**2**), C_{2v} Cs©C_{17}^- (**3**), D_{7h} Na©C_{14}^+ (**4**), C_{2v} Na©C_{13}B (**5**), and C_{2v} Na©C_{13}^- (**6**) are collectively plotted in Fig. 1, with more alternative isomers summarized in Fig. S3–S8.† Fig. S2† depicts the optimized GM structures of (a) the alkaline-metal-centered cyclo[18]carbon complexes M©C_{18}^+ with M = Li, Na, K, Rb, Cs, and Fr and (b) alkaline-metal-centered cyclo[14]carbon complexes M©C_{14}^+ with M = Li, Na, and K at M06-2X. It is noticed that the alkaline metal atoms in the GMs are all located inside the cyclo[*n*]carbon rings, with the alkaline metal atoms severely off-centered in C_{2v} Li©C_{18}^+, C_{2v} Na©C_{18}^+, C_{2v} K©C_{18}^+, and C_{2v} Li©C_{14}^+ and slightly off-centered in C_s Rb©C_{18}^+ and C_s Fr©C_{18}^+. The K atom in C_{7v} K©C_{14}^+ lies about 1.14 Å above the ligand plane along the C_7 molecular axis due to its large atomic radius (r_K = 2.32 Å) which appears to be too big to be hosted inside the C_{14} ring.

Encouragingly, the Cs center with the NBO net atomic charge of q_{Cs} = +0.99 |*e*| proves to have the right atomic radius of r_{Cs} = 2.65 Å to be coordinated exactly at the center of the D_{9h} C_{18} ligand in D_{9h} Cs©C_{18}^+ (**1**) to achieve the highest coordination number of CN = 18 reported to date. As the well-defined GM of the complex (Fig. S3†), Cs©C_{18}^+ (**1**) exhibits the alternating bond lengths of r_{C-C} = 1.343 Å and $r_{C\equiv C}$ = 1.224 Å at M06-2X which are well inherited from its parent ligand D_{9h} C_{18} ligand with r_{C-C} = 1.343 Å and $r_{C\equiv C}$ = 1.223 Å at the same theoretical level (Fig. S1 and Table S1†).

The large calculated HOMO–LUMO gap of ΔE_{gap} = 5.38 eV at M06-2X well supports its high chemical stability. The second isomer C_{2v} Cs©C_{18}^+ with a Cs^+ located outside the C_{18} ring and the seventh isomer C_{2v} Cs©C_{18}^+ with a Cs^+ inserted into the C_{18} ring appear to be 0.38 eV and 4.79 eV less stable than D_{9h} GM at M06-2X, respectively (Fig. S3†). The slightly off-centered planar C_s Rb©C_{18}^+ and C_s Fr©C_{18}^+ also possess the coordination numbers of CN = 18 (Fig. S2†). Both the planar neutral C_s Cs©C_{17}B (**2**) which is isoelectronic with Cs©C_{18}^+ (**1**) with obviously bond-length alternations and C_{2v} Cs©C_{17}^- (**3**) with roughly the same averaged bond lengths are the well-defined GMs of the systems with CN = 18 and 17, respectively (Fig. S4 and S5†). However, the severely off-centered C_{2v} Li©C_{18}^+, C_{2v} Na©C_{18}^+, and C_{2v} K©C_{18}^+ with obvious smaller alkaline metal centers Li, Na, and K appear to have much smaller coordination numbers with CN = 4 ∼ 6 (Fig. S2†).

Similarly, the Na center with q_{Na} = +0.95 |*e*| appears to have the right atomic radius (r_{Na} = 1.86 Å) to be hosted exactly at the center of the D_{7h} C_{14} ligand to form the perfect planar polyynic D_{7h} Na©C_{14}^+ (**4**) (Fig. S6†) with CN = 14. The second lowest-lying isomer C_s Na©C_{14}^+ with the Na^+ center located outside the C_{14} ring lies only 0.23 eV higher than Na©C_{14}^+ (**4**) (Fig. S6†). The two close-lying lowest-lying isomers of Cs©C_{18}^+ and Na©C_{14}^+ discussed above (Fig. S3 and S6†) may transform between each other with low energy barriers under certain conditions. Na©C_{14}^+ (**4**) as the GM of the system has the alternating bond lengths of r_{C-C} = 1.326 Å and $r_{C\equiv C}$ = 1.240 Å at M06-2X well comparable with the corresponding values of r_{C-C} = 1.324 Å and $r_{C\equiv C}$ = 1.237 Å calculated for D_{7h} C_{14} at the same theoretical level (Fig. S1 and Table S1†), while Li with the atomic radius of r_{Li} = 1.52 Å proves to be too small and K with r_K = 2.32 Å appears to be too big to be hosted at the ring center of the C_{14} ligand, they form severely off-centered and off-planed structures, respectively (Fig. S2†). With the HOMO–LUMO gap of ΔE_{gap} = 5.87 eV, Na©C_{14}^+ (**4**) is expected to have a high chemical stability. The slightly off-centered planar C_{2v} Na©C_{13}B (**5**) with CN = 14 and vibrationally averaged C_{2v} Na©C_{13}^- (**6**) with CN = 13 with roughly the averaged bond lengths also appear to be the well-defined GMs of the systems (Fig. S7 and S8†).

As expected, the high-symmetry Cs©C_{18}^+ (**1**) and Na©C_{14}^+ (**4**) exhibit highly characteristic calculated vibrational spectroscopic features as shown in their simulated IR spectra in Fig. S9,† with the former possessing well characterized IR peaks at 513 and 2202 cm^{-1} and Raman active vibrations at 1792 and 2293 cm^{-1}, respectively, while the latter having two well separated IR peaks at 545 and 2160 cm^{-1} and one dominant Raman feature at 1252 cm^{-1}. Such well-defined spectral features can help facilitate future experimental characterizations of these species. Their simulated UV-vis spectra are also shown in Fig. S9† with 100 excited states included to better understand their electronic structures.

3.2 EDA-NOCV bonding scheme analyses

To shed insights into the bonding nature of D_{9h} Cs©C_{18}^+ (**1**) and D_{7h} Na©C_{14}^+ (**4**), detailed EDA-NOCV analyses were carried out at M06-2X/TZ2P. The D_{3h} subgroup was applied to D_{9h} Cs©C_{18}^+ (**1**) because the highest point group supported by ADF program is D_{8h}. It was found that Cs^+ and C_{18} as the most possible reacting fragments give the most favourite orbital interaction energy of ΔE_{orb} = −13.95 kcal mol^{-1} for Cs©C_{18}^+ (**1**) in different fragmental schemes (Table S2†). They are thus chosen as interacting species to demonstrate the bonding scheme of Cs©C_{18}^+ (**1**) in Fig. 2(a). Similarly, Na^+ and C_{14} as reacting fragments with ΔE_{orb} = −22.41 kcal mol^{-1} are chosen for Na©C_{14}^+ (**4**) in Fig. 2(b).

The bonding molecular orbitals (MOs) $15a_1'$, $19e_1'$ and $20e_1'$ of D_{3h} Cs©C_{18}^+ representing covalent bonding MOs between Cs^+ and C_{18} are connected with the corresponding fragmental orbitals by bold dashed lines in Fig. 2(a), with the orbital compositions tabulated in Table S3.† The non-degenerate $15a_1'$ mainly originates from the occupied $8a_1'$ of C_{18} with in-plane π characteristics (abbreviated as π_{in}) and vacant 6s of Cs^+ *via* (π-6s)σ coordination interaction, the doubly degenerate $19e_1'$ is composed of the occupied in-plane $13e_1'$ (π_{in}) of C_{18} with one nodal plane and vacant $7p_x$ and $7p_y$ of Cs^+ *via* (π-7p)σ coordination, while the doubly degenerate $20e_1'$ is composed of the occupied $14e_1'$ of C_{18} with π_{in} characteristics with two nodal planes and vacant $5d_{xy}$ and $5d_{x^2-y^2}$ of Cs^+ *via* (π-5d)σ coordination. As detailed in Table 1, EDA analyses demonstrate that the overall interaction energy of ΔE_{int} = −15.22 kcal mol^{-1} between the Cs^+ and C_{18} in Cs©C_{18}^+ consists of the Pauli repulsion

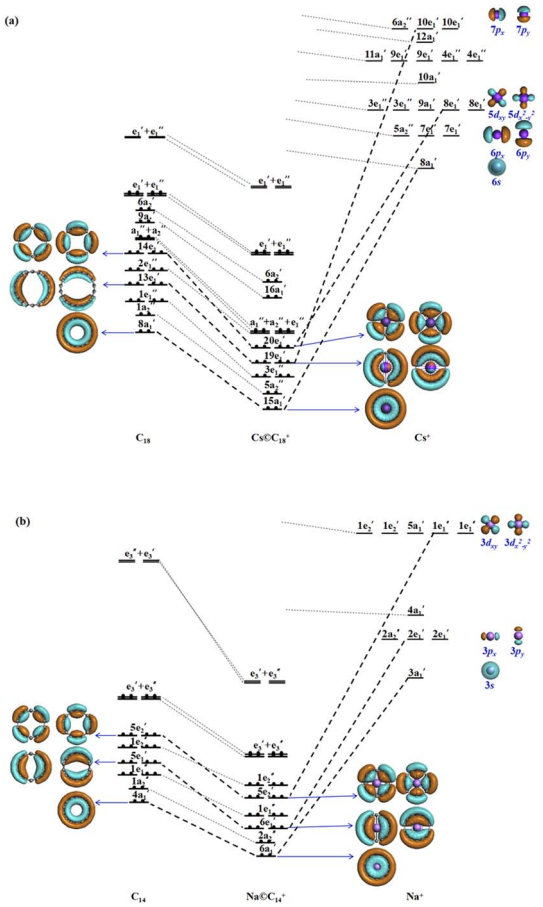

Fig. 2 (a) MO bonding scheme of D_{3h} $Cs©C_{18}^+$ with the fragments of C_{18} and Cs^+ as interacting species and (b) MO bonding scheme of D_{7h} $Na©C_{14}^+$ with C_{14} and Na^+ as interacting species at M06-2X/TZ2P-ZORA level.

ΔE_{Pauli} = 1.89 kcal mol^{-1}, coulombic attraction ΔE_{elstat} = −3.16 kcal mol^{-1}, and orbital interaction ΔE_{orb} = −13.95 kcal mol^{-1}, with covalent orbital interaction making a dominating contribution of 81.5% to the overall attraction interaction (−17.11 kcal mol^{-1}), while electrostatic attraction contributing only 18.5%. The decompositions of the orbital interactions ΔE_{orb} into pairwise contributions between occupied and vacant MOs of the fragments provide quantitative insight into the charge flow. The strongest orbital interaction $\Delta E_{orb(1)}$ (20e$_1'$, 27.5%) arises mainly from [C_{18} (π_{in})] → [Cs^+ (5d)] where C_{18} serves as a π_{in}-donor to coordinate the 5d$_{xy}$ and 5d$_{x^2-y^2}$ orbitals of the Cs^+ as σ-acceptors. The orbital interaction $\Delta E_{orb(2)}$ (19e$_1'$, 16.8%) originates from [C_{18} (π_{in})] → [Cs^+ (7p)] where the 7p$_x$ and 7p$_y$ orbitals of the Cs^+ serve as σ-acceptors. The orbital interaction $\Delta E_{orb(3)}$ (15a$_1'$, 14.1%) originates from [C_{18} (π_{in})] → [Cs^+ (6s)] where the 6s orbital of the Cs^+ is a σ-acceptor. Fig. S10† shows the corresponding deformation densities $\Delta\rho$ associated with the pairwise interactions $\Delta E_{orb(1)}$, $\Delta E_{orb(2)}$ and $\Delta E_{orb(3)}$ in $Cs©C_{18}^+$, further indicating that C_{18} serves as a π_{in}-donor while Cs^+ is a σ-acceptor in the complex.

Detailed EDA-NOCV calculations for D_{7h} $Na©C_{14}^+$ (**4**) gives a similar trend as shown in Fig. 2(b) and Table 1. The bonding MOs 6a$_1'$, 6e$_1'$ and 5e$_2'$ representing covalent bonding interactions between the Na^+ and C_{14} fragmental orbitals are connected by bold dashed lines, with the orbital compositions listed in Table S4.† The 6a$_1'$ mainly originates from the occupied 4a$_1'$ of C_{14} with π_{in} characteristics and vacant 3s of Na^+ *via* (π-3s)σ coordination interaction, the doubly degenerate 6e$_1'$ is composed of occupied 5e$_1'$ of C_{14} with π_{in} characteristics and vacant 3p$_x$ and 3p$_y$ of Na^+ *via* (π-3p)σ coordination, while the 5e$_2'$ is composed of C_{14} with π_{in} characteristics and vacant 3d$_{xy}$ and 3d$_{x^2-y^2}$ of Na^+ *via* (π-3d)σ coordination.

EDA analyses (Table 1) indicate that overall attraction interaction is overwhelmingly dominated by covalent orbital contribution (94.0%), while electrostatic attraction makes only a marginal contribution (6.0%). The decompositions of ΔE_{orb} into pairwise contributions between occupied and vacant MOs of the fragments reveals that the strongest orbital interaction $\Delta E_{orb(1)}$ (24.9%) originates mainly from [C_{14} (π_{in})] → [Na^+ (3p)], the orbital interaction $\Delta E_{orb(2)}$ (19.2%) arises mainly from [C_{14} (π_{in})] → [Na^+ (3s)], while the orbital interaction $\Delta E_{orb(3)}$ (18.1%) originates from [C_{14} (π_{in})] → [Na^+ (3d)]. The corresponding deformation densities $\Delta\rho$ associated with the pairwise interactions $\Delta E_{orb(1)}$, $\Delta E_{orb(2)}$ and $\Delta E_{orb(3)}$ in $Na©C_{14}^+$ in Fig. S11† clearly indicate that C_{14} serves as a π_{in}-donor while Na^+ is a σ-acceptor.

The EDA-NOCV results detailed above quantitatively indicate that the cyclo[4*N* + 2]carbon ligands (*N* = 4, 3) serve as good π_{in}-donors to stabilize alkaline metal centers in both $Cs©C_{18}^+$ (**1**) and $Na©C_{14}^+$ (**4**) by donating their π_{in} valence electrons partially

Table 1 EDA-NOCV results for $Cs©C_{18}^+$ (**1**) and $Na©C_{14}^+$ (**4**) at the M06-2X/TZ2P-ZORA level, taking C_{18} with Cs^+ and C_{14} with Na^+ as interacting fragments, respectively. Energy values are given in kcal mol^{-1}

Energy terms	Interaction	$Cs^+ + C_{18}$	Interaction	$Na^+ + C_{14}$
ΔE_{int}		−15.22		−24.44
ΔE_{elstat}[a]		−3.16 (18.5%)		−1.42 (6.0%)
ΔE_{Pauli}		1.89		3.45
ΔE_{orb}[a]		−13.95 (81.5%)		−22.41 (94.0%)
$\Delta E_{orb(1)}$[b]	C_{18} (π_{in}) donation → [Cs^+ (5d)]	−3.84 (27.5%)	C_{14} (π_{in}) donation → [Na^+ (3p)]	−5.58 (24.9%)
$\Delta E_{orb(2)}$[b]	C_{18} (π_{in}) donation → [Cs^+ (7p)]	−2.34 (16.8%)	C_{14} (π_{in}) donation → [Na^+ (3s)]	−4.30 (19.2%)
$\Delta E_{orb(3)}$[b]	C_{18} (π_{in}) donation → [Cs^+ (6s)]	−1.96 (14.1%)	C_{14} (π_{in}) donation → [Na^+ (3d)]	−4.06 (18.1%)
$\Delta E_{orb(rest)}$[b]		−5.81 (41.6%)		−8.47 (37.8%)

[a] The value in parentheses gives the percentage contribution to the total attractive interactions ($\Delta E_{elstat} + \Delta E_{orb}$). [b] The value in parentheses gives the percentage contribution to the total orbital interaction (ΔE_{orb}).

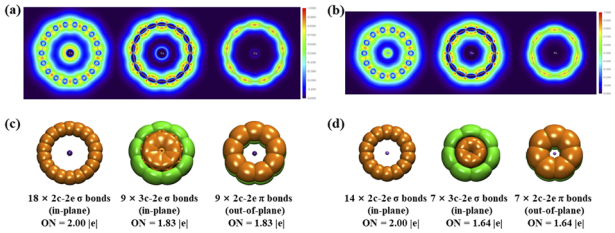

Fig. 3 Color-filled maps of the localized orbital locator isosurfaces of (a) D_{9h} Cs©C_{18}^+ (**1**) and (b) D_{7h} Na©C_{14}^+ (**4**) and AdNDP bonding patterns of (c) D_{9h} Cs©C_{18}^+ (**1**) and (d) D_{7h} Na©C_{14}^+ (**4**) with the occupation numbers (ON) indicated.

to the vacant s, p, and d orbitals of Cs^+ and Na^+ through effective in-plane (π-s)σ, (π-p)σ, and (π-d)σ coordination interactions.

Localized orbital locator (LOL) is an effective space function in revealing the distributions of delocalized electrons on conjugated rings in molecules. We calculated in-plane LOL-σ, in-plane LOL-π_{in}, and out-of-plane LOL-π_{out} separately based on the corresponding in-plane σ MOs, in-plane π MOs, and out-of-plane π MOs of the systems, respectively. To better reflect spatial distributions of LOL-σ, LOL-π_{in}, and LOL-π_{out} in Cs©C_{18}^+ (**1**) and Na©C_{14}^+ (**4**), the color-filled maps of LOL-σ on the ring plane, LOL-π_{in} on the ring plane, and LOL-π_{out} 1 Å above the ring plane are plotted in Fig. 3(a) and (b) comparatively. By comparing the area colors on the maps, it can be clearly seen that both LOL-π_{in} and LOL-π_{out} exhibit heavy density distributions over the short C≡C bonds and light density distributions over the long C–C bonds, well supporting the alternating of triple and single bonds in different bond lengths in both polyynic Cs©C_{18}^+ (**1**) and Na©C_{14}^+ (**4**).

3.3 AdNDP bonding pattern analyses

Detailed AdNDP analyses in Fig. 3(c) and (d) unveil both the localized and delocalized bonds in D_{9h} Cs©C_{18}^+ (**1**) and D_{7h} Na©C_{14}^+ (**4**) more vividly. As expected, out of the 72 valence electrons in Cs©C_{18}^+ (**1**), 36 electrons form 18 equivalent 2c–2e C–C peripheral in-plane σ bonds with the occupation numbers of ON = 2.00 |*e*|. The remaining 36 valence electrons are distributed in two types of chemical bonds, including 9 equivalent in-plane 3c–2e σ bonds on nine CsC_2 triangles with ON = 1.83 |*e*| and 9 equivalent out-of-plane 2c–2e C–C π bonds with ON = 1.83 |*e*|, respectively. Such a bonding pattern follows the $4N + 2$ aromatic rule for σ aromaticity with $N_\sigma = 4$ and π aromaticity with $N_\pi = 4$, respectively, making the planar complex σ + π dually aromatic in nature and rendering extra stability to the system, similar to the situation in the previously reported D_{9h} C_{18}.[11]

Similarly, as shown in Fig. 3(d), D_{7h} Na©C_{14}^+ (**4**) possesses 7 equivalent 2c–2e C–C periphery in-plane σ bonds, 7 equivalent 3c–2e in-plane σ bonds on seven NaC_2 triangles, and 7 equivalent 2c–2e out-of-plane C–C π electrons, again following the $4N + 2$ aromatic rule with $N_\sigma = N_\pi = 3$ for σ + π dual aromaticity. Similar bonding patterns exist in C_s Cs©C_{17}B (**2**) (Fig. S12†). The dual aromaticities of both Cs©C_{18}^+ (**1**) and Na©C_{14}^+ (**4**) are also well supported by numbers of their delocalized in-plane σ MOs and delocalized out-of-plane π MOs shown in Fig. S13.†

The simulated ICSS isosurfaces of D_{9h} Cs©C_{18}^+ (**1**) and D_{7h} Na©C_{14}^+ (**4**) based on the ZZ components of the calculated nuclear-independent chemical shifts (NICS-ZZ) are presented as Fig. 4(a), in comparison with that of the previously reported σ + π dually aromatic D_{9h} C_{18} and D_{7h} C_{14}. It can be clearly seen that, similar to D_{9h} C_{18} and D_{7h} C_{14}, both D_{9h} Cs©C_{18}^+ (**1**) and D_{7h} Na©C_{14}^+ (**4**) are aromatic in nature, with the spaces inside the cyclo[*n*]carbon rings and within ~1.0 Å above the ring planes belonging to chemical shielding areas with negative NICS-ZZ values (highlighted in yellow) and the blet-like regions around the cyclo[*n*]carbon rings in horizontal direction belonging to chemical deshielding areas with positive NICS-ZZ values (highlighted in green).

The widely used ACID method can be employed to display graphically the ring currents induced by an external magnetic

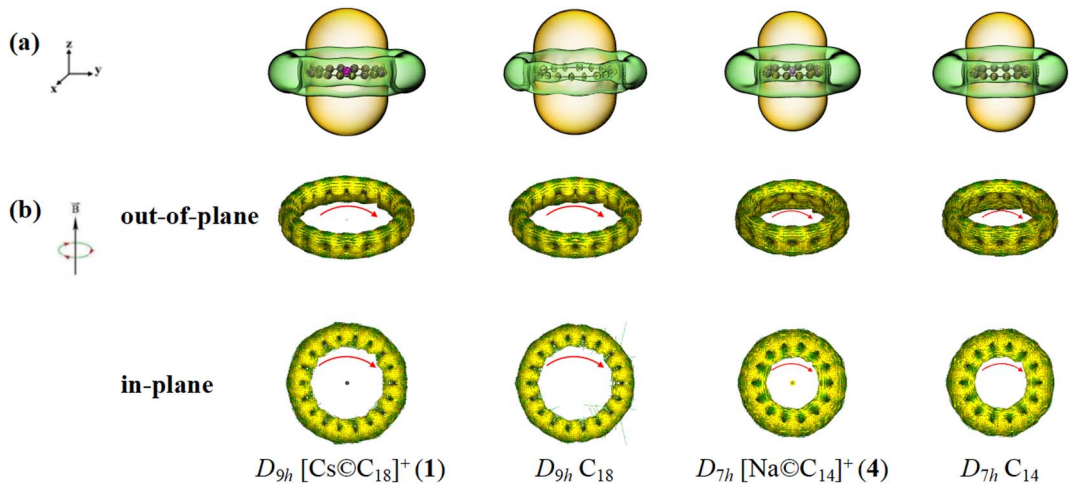

Fig. 4 (a) Calculated iso-chemical shielding surfaces (ICSSs) of D_{9h} Cs©C_{18}^+ (**1**), D_{9h} C_{18}, D_{7h} Na©C_{14}^+ (**4**), and D_{7h} C_{14}. Yellow and green regions stand for chemical shielding and deshielding areas, respectively. (b) Calculated out-of-plane-π and in-plane-σ ring current maps of D_{9h} Cs©C_{18}^+ (**1**) and D_{7h} Na©C_{14}^+ (**4**), compared with the corresponding ring current maps of D_{9h} C_{18} and D_{7h} C_{14}, respectively. The external magnetic field is perpendicular to the ring plane. The red arrows indicate the directions of the ring currents on the ACID iso-surfaces.

field in vertical directions perpendicular to the cyclo[*n*]carbon ring. Fig. 4(b) presents the calculated out-of-plane π and in-plane σ ring currents maps for both D_{9h} $Cs©C_{18}^{+}$ (**1**) and D_{7h} $Na©C_{14}^{+}$ (**4**), in comparison with the corresponding ring currents obtained for D_{9h} C_{18} and D_{7h} C_{14} at the same theoretical level, respectively. As clearly indicated in Fig. 4(b), these alkaline-metal-centered polyynic complex monocations do possess intrinsic σ aromaticity and π aromaticity simultaneously, similar to their neutral parent ligands D_{9h} C_{18} and D_{7h} C_{14} in ring current distributions.

4 Conclusions

In summary, based on extensive first-principles theory calculations, we have predicted in this work a series of alkaline-metal-centered perfect planar complexes $Cs©C_{18}^{+}$ (**1**), $Cs©C_{17}B$ (**2**), $Cs©C_{17}^{-}$ (**3**), $Na©C_{14}^{+}$ (**4**), $Na©C_{13}B$ (**5**), and $Na©C_{13}^{-}$ (**6**) which turn out to be GMs of the systems with the record coordination numbers of CN = 18 ∼ 13 in planar species. These hypercoordinate planar complexes possess effective in-plane (π-s)σ, (π-p)σ, and (π-d)σ coordination interactions which dominate the attractive interaction between the alkaline metal center as σ-acceptor and its cyclo[*n*]carbon ligand as in-plane π-donor, evidencing the transition metal behaviors of the alkaline metal centers in them. Similar to the situation in the recently observed alkaline-earth metal carbonyl species,[21] the proposed perfect planar alkaline-metal-centered polyynic $D_{(2N+1)h}$ cyclo[4*N* + 2]carbon complexes with relatively low coordination energies may be produced in gas phases by laser ablation of alkaline-metal-carbon mixed binary targets and characterized by spectroscopic measurements at low temperatures to further push the boundary of coordination chemistry.

Author contributions

S. D. Li, Z. H. Wei, and Q. Chen conceived the project and finalized the manuscript. M. Z. and R. N. Y. did the calculations and prepared the first draft. Y. B. Wu helped analyze the data. All authors approved the final version.

Conflicts of interest

There are no conflicts to declare.

Acknowledgements

The work was supported by the National Natural Science Foundation of China (21973057, 21720102006 and 22003034) and Natural Science Foundation of Shanxi Province of China (20210302124002).

Notes and references

1 H. W. Kroto, J. R. Heath, S. C. O'Brien, R. F. Curl and R. E. Smalley, *Nature*, 1985, **318**, 162–163.
2 S. Iijima and T. Ichihashi, *Nature*, 1993, **363**, 603–605.
3 K. S. Novoselov, A. K. Geim, S. V. Morozov, D. Jiang, Y. Zhang, S. V. Dubonos, I. V. Grigorieva and A. A. Firsov, *Science*, 2004, **306**, 666–669.
4 K. Kaiser, L. M. Scriven, F. Schulz, P. Gawel, L. Gross and H. L. Anderson, *Science*, 2019, **365**, 1299–1301.
5 G. von Helden, N. G. Gotts and M. T. Bowers, *Nature*, 1993, **363**, 60–63.
6 Y. Rubin, M. Kahr, C. B. Knobler, F. Diederich and C. L. Wilkins, *J. Am. Chem. Soc.*, 1991, **113**, 495–500.
7 A. E. Boguslavskiy, H. Ding and J. P. Maier, *J. Chem. Phys.*, 2005, **123**, 034305.
8 A. E. Boguslavskiy and J. P. Maier, *Phys. Chem. Chem. Phys.*, 2007, **9**, 127–130.
9 T. Torelli and L. Mitas, *Phys. Rev. Lett.*, 2000, **85**, 1702–1705.
10 S. Arulmozhiraja and T. Ohno, *J. Chem. Phys.*, 2008, **128**, 114301.
11 Z. y. Liu, X. Wang, T. Lu, A. h. Yuan and X. f. Yan, *Carbon*, 2022, **187**, 78–85.
12 Y. h. Jiang, Y. b. Wu, J. j. Deng and Z. y Wang, *Phys. Chem. Chem. Phys.*, 2021, **23**, 8817–8824.
13 J. A. Dean, *Lange's Handbook of Chemistry*, McGraw-Hill Book Co., 15th edn, 1999.
14 X. Q. Lu, H. G. Lu and S. D. Li, *RSC Adv.*, 2021, **11**, 27193–27198.
15 T. Heine and G. Merino, *Angew. Chem., Int. Ed.*, 2012, **51**, 4275–4276.
16 T. R. Galeev, C. Romanescu, W. L. Li, L. S. Wang and A. I. Boldyrev, *Angew. Chem., Int. Ed.*, 2012, **51**, 2101–2105.
17 C. Romanescu, T. R. Galeev, W. L. Li, A. I. Boldyrev and L. S. Wang, *Angew. Chem., Int. Ed.*, 2011, **50**, 9334–9337.
18 C. Romanescu, T. R. Galeev, W. L. Li, A. I. Boldyrev and L. S. Wang, *J. Chem. Phys.*, 2013, **138**, 134315.
19 W. L. Li, C. Romanescu, T. R. Galeev, Z. A. Piazza, A. I. Boldyrev and L. S. Wang, *J. Am. Chem. Soc.*, 2012, **134**, 165–168.
20 C. Romanescu, T. R. Galeev, W. L. Li, A. I. Boldyrev and L. S. Wang, *Acc. Chem. Res.*, 2013, **46**, 350–358.
21 X. Wu, L. L. Zhao, J. Y. Jin, S. D. Pan, W. Li, X. Y. Jin, G. J. Wang, M. F. Zhou and G. Frenking, *Science*, 2018, **361**, 912–916.
22 H.-R. Li, X.-Q. Lu, Y.-Y. Ma, Y.-W. Mu, H.-G. Lu, Y.-B. Wu and S.-D. Li, *J. Clust. Sci.*, 2019, **30**, 621–626.
23 J. A. Dean, *Lange's handbook of Chemistry*, McGraw-Hill Book Co, 15th edn, 1999.
24 X. Chen, Y.-F. Zhao, Y.-Y. Zhang and J. Li, *J. Comput. Chem.*, 2019, **40**, 1105–1112.
25 D. J. Wales and H. A. Scheraga, *Science*, 1999, **285**, 1368–1372.
26 J. P. Perdew, K. Burke and M. Ernzerhof, *Phys. Rev. Lett.*, 1996, **77**, 3865.
27 J. VandeVondele, M. Krack, F. Mohamed, M. Parrinello, T. Chassaing and J. Hutter, *Comput. Phys. Commun.*, 2005, **167**, 103–128.
28 Y. Zhao and D. G. Truhlar, *Theor. Chem. Acc.*, 2008, **120**, 215–241.
29 J.-D. Chai and M. Head-Gordon, *Phys. Chem. Chem. Phys.*, 2008, **10**, 6615.

30 D. Feller, *J. Comput. Chem.*, 1996, **17**, 1571–1586.
31 L. Schuchardt, B. T. Didier, T. Elsethagen, L. Sun, V. Gurumoorthi, J. Chase, J. Li and T. L. Windus, *J. Chem. Inf. Model.*, 2007, **47**, 1045–1052.
32 M. J. Frisch, *Gaussian 16, Revision A.03*, Gaussian Inc., Wallingford, CT, 2016.
33 E. D. Glendening, C. R. Landis and F. Weinhold, *J. Comput. Chem.*, 2019, **40**, 2234–2241.
34 T. Ziegler and A. Rauk, *Theor. Chim. Acta*, 1977, **46**, 1–10.
35 M. Mitoraj and A. Michalak, *Organometallics*, 2007, **26**, 6576–6580.
36 M. P. Mitoraj, A. Michalak and T. Ziegler, *J. Chem. Theory Comput.*, 2009, **5**, 962–975.
37 G. te Velde, F. M. Bickelhaupt, E. J. Baerends, C. Fonseca Guerra, S. J. A. van Gisbergen, J. G. Snijders and T. Ziegler, *J. Comput. Chem.*, 2001, **22**, 931–967.
38 E. Van Lenthe and E. J. Baerends, *J. Comput. Chem.*, 2003, **24**, 1142–1156.
39 E. van Lenthe, E. J. Baerends and J. G. Snijders, *J. Chem. Phys.*, 1993, **99**, 4597.
40 D. Y. Zubarev and A. I. Boldyrev, *Phys. Chem. Chem. Phys.*, 2008, **10**, 5207–5217.
41 N. V. Tkachenko and A. I. Boldyrev, *Phys. Chem. Chem. Phys.*, 2019, **21**, 9590–9596.
42 W. Humphrey, A. Dalke and K. Schulten, *J. Mol. Graph.*, 1996, **14**, 33–38.
43 S. Klod and E. Kleinpeter, *J. Chem. Soc., Perkin Trans.*, 2001, **2**, 1893–1898.
44 E. Kleinpeter, S. Klod and A. Koch, *J. Mol. Struct.*, 2007, **811**, 45–60.
45 H. L. Schmider and A. D. Becke, *J. Mol. Struct. (THEOCHEM)*, 2000, **527**, 51–61.
46 T. Lu and F. Chen, *J. Comput. Chem.*, 2012, **33**, 580–592.
47 D. Geuenich, K. Hess, F. Köhler and R. Herges, *Chem. Rev.*, 2005, **105**, 3758–3772.
48 Povray, *Persistence of vision raytracer*, POV-Ray 3.7, **https://www.povray.org/**.